End-capped HyBeacon probes for the analysis of human genetic polymorphisms related to warfarin metabolism†

Nouha Ben Gaied,[a] James A. Richardson,[a] Daniel G. Singleton,[a] Zhengyun Zhao,[a] David French[b] and Tom Brown*[a]

Received 20th January 2010, Accepted 23rd March 2010
First published as an Advance Article on the web 14th April 2010
DOI: 10.1039/c001177k

HyBeacon probes have been used to characterise SNPs in the CYP2C9 and VKORC1 genes associated with variations in the efficiency of warfarin metabolism. PCR amplification of genomic DNA and probe target melting analysis provided a robust and reliable method to differentiate polymorphic sequences at these loci. Probes capped with 5′-trimethoxystilbene were found to exhibit larger fluorescence differences between hybridised and dissociated states than uncapped probes, generating melting peaks of considerably improved height. 3′-Pyrene modifications enhanced probe signal-to-noise and melting peak heights with the additional benefit of acting as PCR stoppers, and 5′,3′-doubly capped probes gave the best analytical results.

Introduction

HyBeacon® probes[1,2] are linear oligonucleotides devoid of secondary structure, possessing one or more fluorescent dyes attached to internal nucleotides and a 3′-blocker to prevent PCR extension of the probe. The inherent fluorescence quenching properties of the DNA bases and attached fluorophores cause the level of fluorescence emission to be low in the single-stranded state. Upon hybridisation to the target DNA sequence, the resultant rigid double-stranded conformation removes the fluorophore from the vicinity of the DNA bases and increases the separation between the dyes. This results in a significant increase in fluorescence, which can be used to discriminate between similar DNA target sequences by melting curve analysis.[3] This is a powerful method of mutation detection particularly as high-resolution DNA melting platforms such as the LightCycler 480®, Rotor-Gene Q and CFX96™ are now available. Unlike many other fluorogenic probes, HyBeacons do not require internal secondary structure for their mode of action, so the melting temperature (T_m) depends only on the degree of homology between the probe and the target sequence, enabling targets with single or multiple polymorphisms to be identified.[4] A key aim in the area of SNP and point mutation analysis is to achieve the greatest possible discrimination between similar sequences, and for this it is desirable to use short probes in order to widen the T_m-gap between allelic variants by increasing the ratio of mismatch to Watson–Crick base pairs. For this to be feasible, suitable methods are required to stabilize short DNA duplexes.

A number of 5′- and internal modifications have previously been incorporated into oligonucleotides to stabilize Watson–Crick duplexes by electrostatic and aromatic stacking on the terminal base pair, among them stilbenes,[5] pyrenes,[6–8] and anthraquinones.[9] Although 5′-stabilization is effective, the use of simple, readily available 3′-stabilizers in genetic probes would be preferable as such modifications will also act as PCR blockers. This negates the need for a separate 3′-phosphate modification, thus simplifying oligonucleotide synthesis by allowing all probes to be assembled from a common solid support. There is a precedent for this in the use of 3′-minor groove binders (MGB probes).[10,11] There is also the possibility of using 5′,3′- dual-modified probes with enhanced DNA-binding properties. To investigate the suitability of these options in the context of HyBeacons we have synthesized several 3′- pyrene and anthraquinone-modified probes, and examined their effects on mismatch discrimination in the presence and in the absence of 5′-trimethoxystilbene (TMS) capping. The same 3′-capping monomers (Fig. 1A, B) have previously been incorporated into oligonucleotides and shown to greatly increase the stability of triplex forming oligonucleotides.[12] This encouraged us to explore their use in HyBeacon probes.

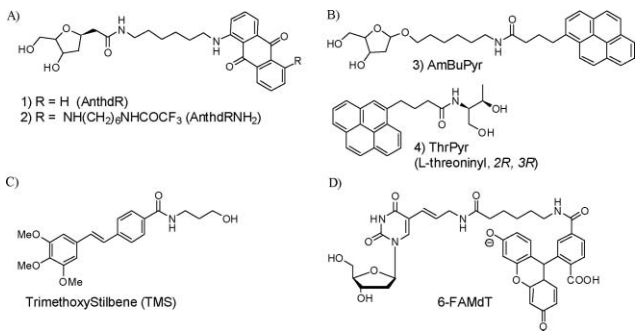

Fig. 1 Chemical structure of oligonucleotide 5′-3′ end caps.

We elected to analyze genes associated with warfarin metabolism to evaluate modified HyBeacons.[13] Warfarin is an important anticoagulant drug that is used to treat and prevent thrombosis. Genetic polymorphisms within the human cytochrome P450 (CYP2C9) and vitamin K epoxide reductase complex subunit 1 (VKORC1) genes are associated with the

[a]*School of Chemistry, University of Southampton, Highfield, Southampton, UK SO17 1BJ. E-mail: tb2@soton.ac.uk; Fax: +44(0)2380 592991; Tel: +44(0)2380 592974*
[b]*Innovation and Development, LGC, Queens Road, Teddington, UK TW11 0LY*

† Electronic supplementary information (ESI) available: Synthetic methods, supplementary figures include UV and fluorescent meltings. See DOI: 10.1039/c001177k

Table 1 PCR primers, probes and oligonucleotide targets. FP: forward primer; RP: reverse primer; MT: matched target: MMT: mismatched target. F = fluorescein dT residue (6-FAM dT)

Oligonucleotides	Sequence
CYP2C9*2 (430 C > T)	
2C9*2-phos	GCATFGAGGACCGFGTTCAAG-P
2C9*2-AnthdR	GCATFGAGGACCGFGTTCAAG-AnthdR
2C9*2-AnthdRNH$_2$	GCATFGAGGACCGFGTTCAAG-AnthdR-NH$_2$
2C9*2-AmBuPyr	GCATFGAGGACCGFGTTCAAG-AmBuPyr
2C9*2-ThrPyr	GCATFGAGGACCGFGTTCAAG-ThrPyr
2C9*2-TMS/phos	TMS-GCATFGAGGACCGFGTTCAAG-P
2C9*2-TMS/AnthdR	TMS-GCATFGAGGACCGFGTTCAAG-AnthdR
2C9*2-TMS/AnthdRNH$_2$	TMS-GCATFGAGGACCGFGTTCAAG-AnthdRNH$_2$
2C9*2-TMS/AmBuPyr	TMS-GCATFGAGGACCGFGTTCAAG-AmBuPyr
2C9*2-TMS/ThrPyr	TMS-GCATFGAGGACCGFGTTCAAG-ThrPyr
2C9*2F2 (**FP**)	GTTTCGTTTCTCTTCCTGTTAGGAATT
2C9*2R2 (**RP**)	GAAGATAGTAGTCCAGTAAGGTCAGTGATATG
2C9*2RC1 (**MT**)	CTTGAACACGGTCCTCAATGC
2C9*2RC2 (**MMT**)	CTTGAACACAGTCCTCAATGC
CYP2C9*3 (1075 A > C)	
2C9*3-phos	TCCAGAGATACCTFGACCTFCTCCC-P
2C9*3-TMS/phos	TMS-TCCAGAGATACCTFGACCTFCTCCC-P
2C9*3F (**FP**)	CATGCAAGACAGGAGCCACAT
2C9*3R (**RP**)	ACAAACTTACCTTGGIAATGAGA
2C9*3RC1 (**MT**)	GGGAGAAGGTCAAGGTATCTCTGGA
2C9*3RC2 (**MMT**)	GGGAGAAGGTCAATGTATCTCTGGA
VKORC1 (-1639 G > A)	
VKORC1-phos	CATFGGCCAGGFGCGGT-P
VKORC1-TMS/phos	TMS-CATFGGCCAGGFGCGGT-P
VKOF1 (**FP**)	GCCAGCAGGAGAGGGAAATA
VKOR2 (**RP**)	GCCTCCCAAAATGCTAGGATT
VKORC1 (**MT**)	ACCGCACCTGGCCAATG
VKORC2 (**MMT**)	ACCGCACCCGGCCAATG

variations in the efficiency of warfarin metabolism.[14–16] Since natural blood clotting is inhibited by this drug, high serum concentrations can cause severe side effects therefore careful monitoring of patients on warfarin medication is critical. In parallel it is important to develop improved methods of screening for genetic variants associated with warfarin metabolism so that patients at risk can be identified at the onset of treatment. Data from SNPs is of real clinical value, as it can be included in dosing algorithms to achieve therapeutic anticoagulation for treatment of arterial and venous thromboembolic disorders.[17] More than 50 single nucleotide polymorphisms (SNPs) have been identified in the regulatory and coding regions of the CYP2C9 gene, and more than 12 allelic genetic variants are known, among them are CYP2C9*1 (Arg^{144}/Ile^{359}), CYP2C9*2 (Cys^{144}/Ile^{359}) and CYP2C9*3 (Arg^{144}/Leu^{359}).[14,18] The single amino acid replacement that is present in CYP2C9*3 is known to be involved in significant changes in substrate affinity, while the effects of CYP2C9*2 are not well determined.

Results and discussion

Several probes, each with two internal fluorescein dT (6-FAM dT) residues, were designed to interrogate polymorphic CYP2C9 or VKORC-1 target sequences (Table 1).

Probes were either uncapped, 5′-capped with TMS, 3′-capped with anthraquinone or pyrene derivatives, or capped at both 5′ and 3′-ends (Fig. 1). Previous work has demonstrated the advantage of using HyBeacon probes containing two fluorescent dyes rather than single-labelled probes,[4] as the former results in much less fluorescence in the (dark) single-strand due to fluorophore-fluorophore quenching. This produces probes with increased signal-to-noise ratios and improved melting peak heights.

Polymorphic target sequences are detected through melting peak analysis, using melting temperatures (T_ms) to identify the alleles present. The 2C9*2 probes were designed to analyse the CYP2C9 430 C > T polymorphism (rs1799853) and possess a C nucleotide at the polymorphic site, generating higher T_m melting peaks with the complementary 'wild-type' (CYP2C9*1) allele compared with the CYP2C9*2 target which produces a C/A mismatch. Samples of *1/*2 genotype generate both matched and mismatched melting peaks.

2C9*3 probes were designed to analyse the CYP2C9 1075 A > C polymorphism (rs1057910) and possess a C nucleotide at the polymorphic site, generating higher melting peaks with the complementary *3 allele compared with the 'wild-type' *1 sequence which exhibits a C/T mismatch. Samples of *1/*3 genotype yield both matched and mismatched melting peaks. Samples that generate *2 and *3 melting peaks with the above tests are typed as *2/*3. VKORC1 probes were designed to analyse the -1639 G > A polymorphism (rs9923231) and are complementary to target sequences possessing T at the polymorphic site, generating melting peaks of reduced T_m when hybridized to the C target variant.

Before commencing the PCR and genotyping analysis of the end-capped probes, we measured their fluorescence properties (Table 2). The individual anthraquinones 1 and 2, and pyrenes 3 and 4 (Fig. 1) exhibit low fluorescence with excitation and emission wavelengths well separated from those of fluorescein. This is important, as these monomers are not intended to behave

Table 2 UV and fluorescence melting of 2C9*2 HyBeacon probes with matched and mismatched oligonucleotide targets. End modifications in Fig. 1. Oligonucleotide sequences in Table 1. Matched target = 2C9*2RC1 with CG base pair, mismatched target = 2C9*2RC2 with CA mismatch

	Fluorescence melting		UV melting	Quantum yield	
End mods 5′- 3′	T_m/°C[a]	T_m/°C[b]	T_m/°C[c]	Single strand	Double strand
Phos	67.5/58.7	58.8/55.3	62.4/54.5	0.219	0.807
AnthdR	73.1/64.3	62.3/54.6	65.0/56.9	0.067	0.242
AnthdRNH$_2$	71.9/63.0	60.6/53.3	63.8/55.4	0.054	0.233
AmBuPyr	73.0/64.5	61.7/56.1	64.9/57.1	0.318	0.902
ThrPyr	73.6/65.2	62.2/56.4	65.4/57.2	0.281	0.773
TMS-phos	68.3/59.7	60.1/55.9	63.8/55.8	0.214	0.616
TMS-AnthdR	74.0/65.4	63.2/56.1	65.8/57.8	0.054	0.274
TMS-AnthdRNH$_2$	72.5/63.6	61.4/53.5	64.6/56.1	0.053	0.199
TMS-AmBuPyr	74.1/65.7	62.8/56.5	66.1/57.9	0.286	0.958
TMS-ThrPyr	74.7/66.3	63.3/56.8	66.5/58.7	0.245	0.890

[a] TaKaRa PCR buffer pH 8.3, 1 M NaCl. [b] 10 mM Na_2HPO_4/NaH_2PO_4 buffer, 200 mM NaCl, pH 7. [c] 10 mM Na_2HPO_4/NaH_2PO_4 buffer, 200 mM NaCl, pH 7.

Table 3 Comparison of 5′ and 3′-capped probes with oligonucleotide targets. 1 × TaKaRa PCR buffer containing 1 M NaCl, pH 8.3 (TaKaRa Bio Inc.)

Probe cap	Target	N	T_m/°C	Area	Height	S/N
Uncapped	A	6	50.1	2.6	0.4	1.3
	G	6	57.7	7.8	0.9	1.9
TMS	A	6	52.6	5.4	1.0	2.3
	G	6	60.8	10.4	1.8	3.5
3′-AnthdR	A	6	51.0	2.1	0.4	2.1
	G	6	59.6	3.2	0.5	2.8
3′ AnthdRNH$_2$	A	6	49.1	1.6	0.3	2.1
	G	6	58.0	2.4	0.4	2.8
3′-AmBuPyr	A	6	51.3	3.7	0.6	1.7
	G	6	59.5	8.6	1.4	2.7
3′-ThrPyr	A	6	51.2	3.9	0.7	1.6
	G	6	59.4	10.3	1.7	2.5

as fluorophores, but as PCR stoppers and duplex stabilizers. To evaluate the effect of the end-caps on fluorescence, we measured the quantum yields of probes in single and double-stranded states at the excitation and emission wavelengths of fluorescein (Table 2).

A decrease of the overall fluorescence quantum yield relative to the uncapped probe was observed with anthraquinones at the 3′-end of single-stranded oligonucleotides, presumably due to FRET or electron transfer between fluorescein and the anthraquinone chromophores, with a smaller but significant decrease in the double-stranded state. This quenching was also observed by fluorescence melting curve analyses through the generation of melting peaks of reduced height (Fig. 2B, Table 3).

In contrast, when 3′-pyrenes were used, either in single or double-stranded DNA, no reduction was observed in the quantum yield and melting peak heights compared to the uncapped probe; in fact there was a slight increase in both. The 3′-ThrPyr and 5′-TMS caps provided similar improvements to the sharpness (inverse of width) and intensity (height) of melting peaks relative to the uncapped probe (Fig. 2A). We also systematically evaluated the effects of the end-caps for their ability to increase duplex melting temperature against single-stranded oligonucleotide targets (Tables 2 and 3). The 2C9*2 probes were evaluated using oligonucleotides which were fully complementary (2C9*2RC1) or

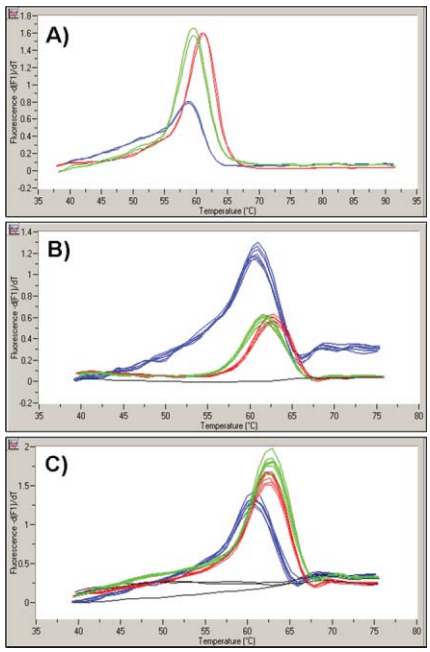

Fig. 2 (A) Comparison of uncapped (blue), 5′-TMS capped (red) and 3′-ThrPyr capped (green) CYP2C9*2 probe melting peaks with oligonucleotide targets. (B) Comparison of uncapped (blue), 3′-AnthdR capped (red) and 3′-AnthdR-NH$_2$ capped (green) probes with PCR amplified targets. (C) Comparison of uncapped (blue), 3′-AmBuPyr (red) and 3′-ThrPyr (green) capped probes with PCR amplified targets. No-template controls in black. LightCycler®, excitation at 470 nm.

possessed a single nucleotide mismatch (2C9*2RC2). Fluorescence and ultraviolet melting was measured in buffers of varying salt composition and pH (500 mM, 200 mM NaCl at pH 7, 8.1 and 8.7). The modifications generally produced a slight increase in T_m.

Next we compared the uncapped and 5′-TMS-capped 2C9*2, 2C9*3 and VKORC1 probes using oligonucleotide targets and melting curve analysis performed with a LightCycler® instrument (Table 4). The melting peak heights, areas, T_m values and signal-to-noise were all increased relative to the uncapped probes. The

Table 4 Melting curve analysis of 5′-trimethoxystilbene capped probes with oligonucleotide targets (where N is the number of melting peaks analysed and S/N the signal-to-noise ratio). 1 × TaKaRa PCR buffer containing 1 M NaCl, pH 8.3 (TaKaRa Bio Inc.)

Probe	Target	N	Peak T_m/°C	Area	Height	S/N
C9*2	A (*2)	6	50.6	2.2	0.3	1.4
	G (*1)	6	57.9	6.3	0.7	2.0
C9*2TMS	A (*2)	6	53.0	6.3	0.9	2.2
	G (*1)	6	60.9	11.7	1.7	3.4
2C9*3	T (*1)	6	54.9	5.1	0.6	1.4
	G (*3)	6	61.9	5.1	0.6	1.5
2C9*3TMS	T (*1)	6	57.4	7.6	1.0	1.6
	G (*3)	6	64.2	7.4	0.9	1.7
VKORC1	C	6	48.4	8.9	1.0	2.0
	T	6	58.4	8.7	0.9	2.2
VKORC1TMS	C	6	52.6	12.7	1.5	4.1
	T	6	61.3	13.0	1.5	4.3

3′-pyrene probes performed in a similar manner to the TMS probes (Table 3).

A series of asymmetric PCR amplifications and post-PCR melting experiments were then performed. These assays generated an excess of the target DNA strand, limiting the amount of complementary strand that would compete for probe hybridisation. The TMS caps increased the amount of fluorescent signal generated during target amplification, possibly by improving the thermodynamics and kinetics of probe-target binding, but it did not change the cycle threshold at which target amplification was detected (Fig. 3).

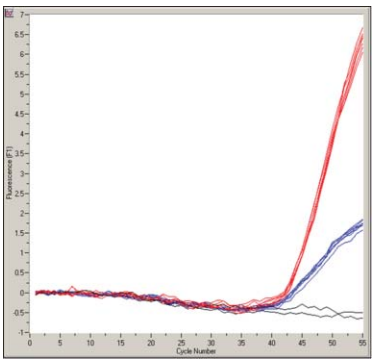

Fig. 3 Real time PCR analysis of 2C9*2-phos (blue) and 2C9*2-TMS/phos (red) probes. The TMS cap increases the fluorescence signal generated during amplification without affecting the cycle threshold of detection. No-template controls are presented (black).

The melting peak heights and areas of TMS capped probes were improved relative to the uncapped probes (Fig. 4, Table 5), and this increased the ability of the analysis software to detect and identify target alleles. The uncapped 2C9*3 probe generated small mismatched melting peaks (Fig. 4B) and analysis software occasionally failed to detect the allele with a small number (<1%) of samples of *1/*3 genotype, yielding an incorrect *3/*3 call.

The improved peak height generated with the 2C9*3TMS capped probe ensures assay accuracy and robustness.

When 3′-capped probes were used in PCR amplification, anthraquinone analogues generated melting peaks of reduced height and area compared with the uncapped probe (Fig. 2B, Table 6), whereas the AmBuPyr and ThrPyr caps increased the heights and areas of melting peaks (Fig. 2C, Table 6). As with

Table 5 Melting curve analysis of 5′-trimethoxystilbene capped probes and PCR amplified targets

Probe	Target	N	T_m/°C	Area	Height
C9*2	G	7	59.9	7.4	1.0
C9*2TMS	G	7	61.4	10.9	1.8
2C9*3	T	7	56.4	0.4	0.4
	G	7	64.4	1.4	0.6
2C9*3TMS	T	7	58.9	2.1	0.6
	G	7	66.0	3.4	1.1
VKORC1	C	7	48.4	7.2	1.1
	T	7	58.4	7.1	1.1
VKORC1TMS	C	7	51.9	11.2	1.8
	T	7	60.7	9.5	1.6

Table 6 Melting curve analysis of 3′-capped probes and PCR amplified targets (where N is the number of melting peaks analysed).

Probe cap	Target	N	T_m/°C	Area	Height
Uncapped	G	14	60.4	9.8	1.3
3′-AnthdR	G	7	62.6	3.4	0.6
3′-AnthdRNH$_2$	G	7	61.6	3.6	0.6
3′-AmBuPyr	G	7	62.2	11.2	1.6
3′-ThrPyr	G	7	62.5	12.7	1.8

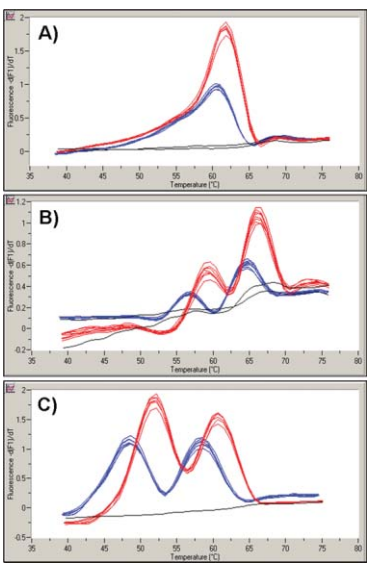

Fig. 4 (**A**) Melting curve analysis of 2C9*2-phos (blue) and 2C9*2-TMS/phos (red) probes with PCR-amplified targets. (**B**) Melting curve analysis of 2C9*3-phos (blue) and 2C9*3-TMS/phos (red) probes with heterozygous DNA samples. (**C**) Melting curve analysis of VKORC1-phos (blue) and VKORC1-TMS/phos (red) probes with heterozygous DNA samples. Seven replicate positive controls and two No-template controls (black) were analysed for each capped and uncapped probe. LightCycler®, excitation at 470 nm.

TMS, none of the 3′-caps had an effect on cycle threshold. The 3′-ThrPyr cap provides the best alternative to 5′-TMS, exhibiting equivalent improvements to melting peak height, with the added benefit that the 3′-cap modification replaces the 3′-phosphate typically employed to prevent PCR extension from probes.

Probes capped at both 5′ and 3′ ends were also found to enhance the fluorescence difference between hybridised and dissociated probe states, increasing the heights and areas of melting peaks. The 2C9*2 probes capped at the 5′ end with TMS and at the

Table 7 Properties of HyBeacon probes capped at both 5′ and 3′ ends (where N is the number of melting peaks analysed and S/N the signal-to-noise ratio).

Probe cap	Target	N	Area	T_m/°C	Height	S/N	ΔT_m/°C
Uncapped	A	6	2.2	50.4	0.3	1.3	
	G	6	6.7	58.0	0.8	2.0	
TMS	A	6	4.8	53.0	0.9	2.3	2.6
	G	6	9.2	61.1	1.5	3.5	3.1
TMS-AnthdR	A	6	2.2	53.5	0.4	3.0	3.1
	G	6	3.0	61.9	0.5	3.6	3.9
TMS-AnthdRNH$_2$	A	6	1.4	51.5	0.2	2.6	1.2
	G	6	2.0	60.3	0.3	3.1	2.2
TMS-AmBuPyr	A	6	4.9	53.8	0.8	2.2	3.5
	G	6	9.0	62.0	1.5	3.5	3.9
TMS -ThrPyr	A	6	5.5	53.8	0.9	2.5	3.4
	G	6	10.2	62.0	1.8	3.9	4.0

3′ end with AmBuPyr or ThrPyr provided a small T_m and peak height increase with oligonucleotide targets compared with the probe capped with TMS only (Table 7, Fig. 5A). The improvement to peak heights, however, was not as pronounced with PCR-amplified targets (Fig. 5B), although the dual-capped probes did produce the highest melting temperatures. As anticipated, the 2C9*2 probes capped at the 5′-end with TMS and at the 3′-end with AnthdR or AnthdRNH$_2$ generated melting peaks of reduced height compared with the probe capped with TMS only (Table 7). The reduced performance of AnthdR and AnthdRNH$_2$ probes is likely to be due to FRET-based quenching of fluorescein by the anthraquinone chromophore, which, unlike pyrene, absorbs at the excitation frequency of fluorescein (UV/visible spectra in the ESI†).

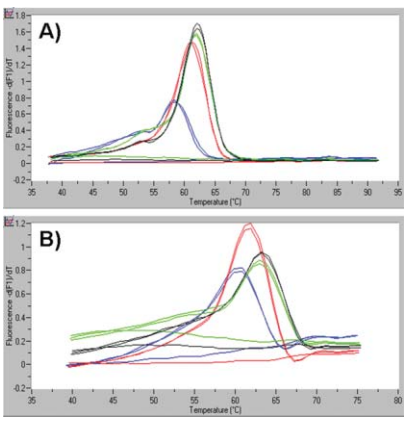

Fig. 5 Comparison of 2C9*2-phos (blue), 2C9*2-TMS/phos (red), 2C9*2 TMS/AmBuPyr (green) and 2C9*2-TMS/ThrPyr probes (black). Melting curve analysis was performed with (A) oligonucleotide and (B) PCR-amplified targets. No-template controls are presented. LightCycler®, excitation at 470 nm.

Oligonucleotide probes melt in a non-cooperative manner, as the termini dissociate from the target earlier than central regions due to ingress of water. Stabilizing the probe by 5′- or 3′-capping with aromatic groups prevents "end-fraying" of duplexes and increase probe T_m. It also increases the signal of hybridised probes relative to uncapped oligonucleotides of identical sequence, yielding probes with melting peaks of increased height

Conclusions

End-capped HyBeacons have been developed to reliably genotype single nucleotide polymorphisms associated with warfarin metabolism by melting curve analysis. Probe melting temperatures, signal-to-noise ratios and melting peak heights are enhanced using 5′ and 3′-cap modifications, increasing the efficiency, accuracy and robustness of the assay. This is likely to be of benefit in the analysis of unpurified clinical samples (such as saliva, swabs and blood), which may yield melting peaks of reduced height compared with extracted DNA due to low DNA concentrations and the presence of PCR inhibitors.[2,4] Clinical decisions could be made on the basis of the assay results, so a high level of reliability is important. End-cap modifications are now routinely used by us, and are particularly useful with target sequences that form secondary structures which would otherwise prevent efficient probe hybridisation. The 3′-caps have the additional benefit of acting as PCR stoppers and can be used in place of 3′ phosphate.

Experimental

DNA phosphoramidite monomers, solid supports including phosphate-on synthesis columns, and additional reagents were purchased from Link Technologies Ltd or Applied Biosystems Ltd. Anthraquinone and pyrene analogues for 3′-oligonucleotide modification (Fig. 1) and the corresponding oligonucleotide synthesis resins were prepared as described previously.[12] Human genomic DNA for the PCR experiments was sourced from Gentris products, distributed by LGC Standards.

Determination of quantum yields

Quantum yields of fluorescein were calculated at an optical density of 0.01 at the excitation wavelength of 460 nm for modified HyBeacons®. A standard of fluorescein in 0.1 M NaOH was used for quantum yield determination of oligonucleotides which were dissolved in 10 mM Na_2HPO_4/NaH_2PO_4 buffer (pH 8) containing 100 mM NaCl. Emission spectra were recorded using a Perkin Elmer LS 50B luminescence spectrometer fitted with a Perkin Elmer PTP1 Peltier temperature control device using a 90° collection angle.

Oligonucleotide synthesis and purification

Oligonucleotide synthesis was carried out on an Applied Biosystems 394 automated DNA/RNA synthesizer using standard 0.2 μmol and 1.0 μmol phosphoramidite cycles of acid-catalyzed detritylation, coupling, capping and iodine oxidation. All β-cyanoethyl phosphoramidite monomers were dissolved in anhydrous acetonitrile to a concentration of 0.1 M immediately prior to use. The coupling time for normal A, G, C and T monomers was 25 s, and this was extended to 10 min for fluorescein-dT (FAM) and trimethoxystilbene (TMS), purchased from Link Technologies Ltd and Glen Research respectively. For resins functionalized with L-threoninol derivatives, coupling of the first monomer to the solid support was carried out for 5 min to ensure an efficient reaction at this hindered site. Stepwise coupling efficiencies and overall yields were determined by automated trityl cation conductivity monitoring and in all cases were >98.0%. Cleavage of oligonucleotides from the solid support and deprotection were achieved by exposure

to concentrated aqueous ammonia for 60 min at room temperature followed by heating in a sealed tube for 5 h at 55 °C. Purification of oligonucleotides was carried out by reversed-phase HPLC on a Gilson system using a Brownlee Aquapore column (C8, 8 mm × 250 mm, 300 Å pore) with a gradient of acetonitrile in ammonium acetate increasing from 0% to 50% buffer B over 30 min with a flow rate of 4 mL min^{-1} (buffer A: 0.1 M ammonium acetate, pH 7.0, buffer B: 0.1 M ammonium acetate with 50% acetonitrile pH 7.0). Elution of oligonucleotides was monitored by ultraviolet absorption at 295 nm. After HPLC purification, oligonucleotides were desalted using NAP-10 Sephadex columns (GE Healthcare) according to the manufacturer's instructions.

Ultraviolet melting studies

To determine duplex melting temperatures (T_m), UV melting studies were carried on a Varian Cary 400 scan UV-visible spectrophotometer using Hellma SUPRASIL synthetic quartz 10 mm path length cuvettes, monitoring at 260 nm with a DNA single strand concentration of 1.0 µM and a volume of 1.2 mL. Samples were prepared as follows: single strand of the target and probe were mixed in a 1 : 1 ratio (concentrations determined by UV absorbance and extinction coefficients) in 2 mL Eppendorf tubes then lyophilized before resuspending in 1.2 mL in 10 mM phosphate buffer, 200 mM or 500 mM NaCl at pH 7.0 and finally filtered through Kinesis cellulose 13 mm diameter 0.45 µM syringe filters. The UV melting protocol involved initial denaturation by heating to 80 °C at 10 °C min^{-1} followed by an annealing step cooling to 20 °C at 0.5 °C min^{-1}. The temperature was maintained at 20 °C for 20 min before starting the melting experiment which involved heating from 20 °C to 80 °C at 0.5 °C min^{-1}, holding at 80 °C for two min, then cooling to 20 °C at 0.5 °C min^{-1}. Two successive melting curves were measured before rapid annealing from 80 °C to 20 °C at 10 °C min^{-1}. T_m values were calculated using Cary Win UV thermal application software, taking an average of the two melting curves.

Fluorescence melting studies on probe-target duplexes

Fluorescence melting curves in Table 2 were determined using a Roche LightCycler® with a total reaction volume of 20 µL. For each oligonucleotide the final concentration was 0.25 µM in 10 mM sodium phosphate buffer, pH 7.0 varying the salt concentration (500 or 200 mM NaCl) with a ratio of 1.5 : 1.0 target to probe. Fluorescence melting curves were also measured in 1 × TaKaRa PCR buffer containing 1M NaCl, pH 8.3 (TaKaRa Bio Inc.) Samples were first denaturated by heating to 95 °C at a rate of 20 °C min^{-1} and maintained at this temperature for 5 min before annealing by cooling to 35 °C at 0.1 °C s^{-1}. Samples were then held at 35 °C for a further 5 min then melted by heating to 95 °C at 0.1 °C s^{-1}. Experiments were performed in duplicate and T_m values were calculated using Light Cycler software (version 3.5), taking an average of the two melting curves. For the data in Tables 3, 4 and 7, 10 µL reaction volumes were used, containing 1× QIAGEN PCR buffer, a total of 3 mM MgI_2, 150 nM fluorescent probe, 150 nM target oligonucleotide and 10 ng $µL^{-1}$ BSA (Roche Diagnostics, Lewes, UK). Following a denaturation (95 °C, 15 s) and cooling (35 °C, 30 s), samples were heated to 95 °C at 0.2 °C per second.

PCR amplification and melting curve analysis

PCR volumes were 20 µL, containing 2 µL purified human DNA (between 1–10 ng $µL^{-1}$ concentration), 1× QIAGEN PCR buffer, 1 unit HotStarTaq polymerase (QIAGEN, Crawley, UK), 1 mM dNTPs (0.25 mM each—GE Healthcare, Amersham, UK), 0.1 µM forward primer, 0.5 µM reverse primer, 150 nM probe and 10 ng $µL^{-1}$ BSA (Roche Diagnostics, Lewes, UK). The sequences of primers, probe and blocker oligonucleotides are detailed in Table 1. Asymmetric PCR was used to generate an excess of the target strand such that probe hybridisation was favoured over annealing of amplified sequences. Amplification of target sequences was performed using a LightCycler® instrument. Following an initial denaturation to activate the hotstart enzyme (95 °C, 15 min), targets were amplified using 55 cycles comprising denaturation (95 °C, 5 s), primer annealing (55 °C, 10 s) and extension of products (72 °C, 15 s). Following amplification, reactions were incubated at 72 °C for 2 min prior to a denaturation (95 °C, 30 s) and cool (35 °C, 1 min) steps. Melting curve analysis was performed by heating from 35 °C to 80 °C, at 0.2 °C per second. The T_ms and areas of melting peaks were obtained using version 3.5 of LightCycler® software. Peak height was determined as the maximum −dF/dT value from exported melting peak data and signal-to-noise ratio (S/N) was calculated using exported melting curve data, as the fluorescence at T_m − 10 °C divided by the fluorescence at T_m + 10 °C.

Acknowledgements

This project was supported by the European Commission's Sixth framework Programme (Project reference ZNIP) [037783] and an EPSRC research studentship to JAR. Oligonucleotide synthesis was carried out by ATDBio Ltd.

Notes and references

1 D. J. French, C. L. Archard, T. Brown and D. G. McDowell, *Mol. Cell. Probes*, 2001, **15**, 363–374.
2 D. J. French, C. L. Archard, M. T. Andersen and D. G. McDowell, *Mol. Cell. Probes*, 2002, **16**, 319–326.
3 A. H. R. Marks, P. K. Bhadra, D. G. McDowell, D. J. French, K. T. Douglas, E. V. Bichenkova and R. A. Bryce, *J. Biomol. Struct. Dyn.*, 2005, **23**, 49–62.
4 D. J. French, D. Jones, D. G. McDowell, J. A. Thomson and P. G. Debenham, *BMC Infect. Dis.*, 2007, **7**, 90.
5 Z. Dogan, R. Paulini, J. A. R. Stutz, S. Narayanan and C. Richert, *J. Am. Chem. Soc.*, 2004, **126**, 4762–4763.
6 V. V. Filichev and E. B. Pedersen, *Org. Biomol. Chem.*, 2003, **1**, 100–103.
7 U. B. Christensen and E. B. Pedersen, *Nucleic Acids Res.*, 2002, **30**, 4918–4925.
8 V. V. Filichev and E. B. Pedersen, *J. Am. Chem. Soc.*, 2005, **127**, 14849–14858.
9 K. Mori, C. Subasinghe and J. S. Cohen, *FEBS Lett.*, 1989, **249**, 213–218.
10 E. A. Lukhtanov, I. V. Kutyavin, H. B. Gamper and R. B. Meyer, *Bioconjugate Chem.*, 1995, **6**, 418–426.
11 I. V. Kutyavin, I. A. Afonina, A. Mills, V. V. Gorn, E. A. Lukhtanov, E. S. Belousov, M. J. Singer, D. K. Walburger, S. G. Lokhov, A. A. Gall, R. Dempcy, M. W. Reed, R. B. Meyer and J. Hedgpeth, *Nucleic Acids Res.*, 2000, **28**, 655–661.
12 N. Ben Gaied, Z. Y. Zhao, S. R. Gerrard, K. R. Fox and T. Brown, *ChemBioChem*, 2009, **10**, 1839–1851.

13 U. Yasar, E. Eliasson, M. L. Dahl, I. Johansson, M. Ingelman-Sundberg and F. Sjoqvist, *Biochem. Biophys. Res. Commun.*, 1999, **254**, 628–631.
14 A. E. Rettie, L. C. Wienkers, F. J. Gonzalez, W. F. Trager and K. R. Korzekwa, *Pharmacogenetics*, 1994, **4**, 39–42.
15 D. J. Steward, R. L. Haining, K. R. Henne, G. Davis, T. H. Rushmore, W. F. Trager and A. E. Rettie, *Pharmacogenetics*, 1997, **7**, 361–367.
16 S. Rost, A. Fregin, V. Ivaskevicius, E. Conzelmann, K. Hortnagel, H. J. Pelz, K. Lappegard, E. Seifried, I. Scharrer, E. G. D. Tuddenham, C. R. Muller, T. M. Strom and J. Oldenburg, *Nature*, 2004, **427**, 537–541.
17 E. A. Sconce, T. I. Khan, H. A. Wynne, P. Avery, L. Monkhouse, B. P. King, P. Wood, P. Kesteven, A. K. Daly and F. Kamali, *Blood*, 2005, **106**, 2329–2333.
18 H. Takahashi and H. Echizen, *Clin. Pharmacokinet.*, 2001, **40**, 587–603.

